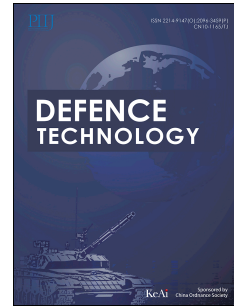


# Journal Pre-proof

Construction of core@double-shell structured energetic composites with simultaneously enhanced thermal stability and safety performance

Peng Wang, Wen Qian, Ruolei Zhong, Fangfang He, Xin Li, Jie Chen, Li Meng, Yinshuang Sun, Guansong He



PII: S2214-9147(23)00299-4

DOI: <https://doi.org/10.1016/j.dt.2023.11.011>

Reference: DT 1357

To appear in: *Defence Technology*

Received Date: 22 August 2023

Revised Date: 3 October 2023

Accepted Date: 6 November 2023

Please cite this article as: Wang P, Qian W, Zhong R, He F, Li X, Chen J, Meng L, Sun Y, He G, Construction of core@double-shell structured energetic composites with simultaneously enhanced thermal stability and safety performance, *Defence Technology* (2023), doi: <https://doi.org/10.1016/j.dt.2023.11.011>.

This is a PDF file of an article that has undergone enhancements after acceptance, such as the addition of a cover page and metadata, and formatting for readability, but it is not yet the definitive version of record. This version will undergo additional copyediting, typesetting and review before it is published in its final form, but we are providing this version to give early visibility of the article. Please note that, during the production process, errors may be discovered which could affect the content, and all legal disclaimers that apply to the journal pertain.

© 2023 China Ordnance Society. Publishing services by Elsevier B.V. on behalf of KeAi Communications Co. Ltd.

## **Construction of core@double-shell structured energetic composites with simultaneously enhanced thermal stability and safety performance**

Peng Wang <sup>a</sup>, Wen Qian <sup>a</sup>, Ruolei Zhong <sup>a</sup>, Fangfang He <sup>b</sup>, Xin Li <sup>a</sup>, Jie Chen <sup>a</sup>, Li Meng <sup>a</sup>, Yinshuang Sun <sup>a</sup>, Guansong He <sup>a,\*</sup>

<sup>a</sup> Institute of Chemical Materials, China Academy of Engineering Physics, Mianyang 621900, China

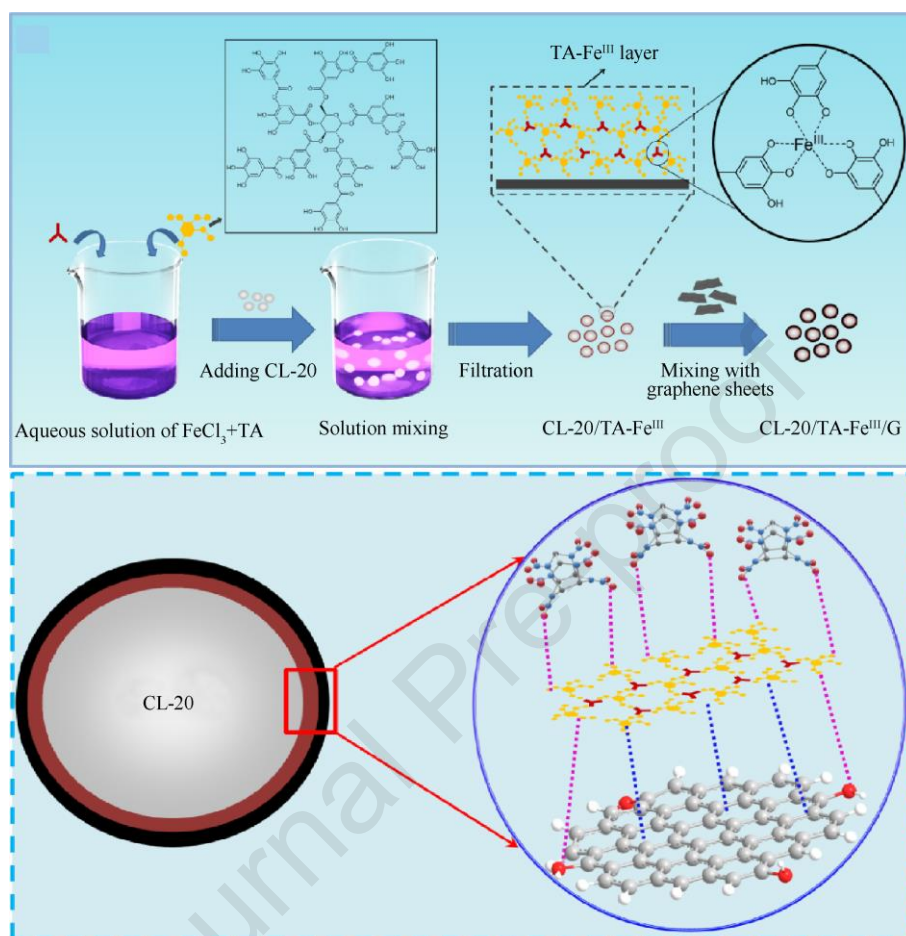
<sup>b</sup> State Key Laboratory of Environment-friendly Energy Materials, School of Materials and Chemistry, Southwest University of Science and Technology, Mianyang, 621010, China

**\*Corresponding author:** Guansong He

E-mail: heguansong@caep.cn

Journal Pre-proof

**Construction of core@double-shell structured energetic composites with simultaneously enhanced thermal stability and safety performance**



Graphical abstract

## Construction of core@double-shell structured energetic composites with simultaneously enhanced thermal stability and safety performance

### Abstract

The poor thermal stability and high sensitivity severely hinder the practical application of hexanitrohexaazaisowurtzitane (CL-20). Herein, a kind of novel core@double-shell CL-20 based energetic composites were fabricated to address the above issues. The coordination complexes which consist of natural polyphenol tannic acid (TA) and Fe<sup>III</sup> were chosen to construct the inner shell, while the graphene sheets were used to build the outer shell. The resulting CL-20/TA-Fe<sup>III</sup>/graphene composites exhibited simultaneously improved thermal stability and safety performance with only 1 wt% double-shell content, which should be ascribed to the intense physical encapsulation effect from inner shell combined with the desensitization effect of carbon nano-materials from outer shell. The phase transition ( $\epsilon$  to  $\gamma$ ) temperature increased from 173.70 °C of pure CL-20 to 191.87 °C of CL-20/TA-Fe<sup>III</sup>/graphene composites. Meanwhile, the characteristic drop height ( $H_{50}$ ) dramatically increased from 14.7 cm of pure CL-20 to 112.8 cm of CL-20/TA-Fe<sup>III</sup>/graphene composites, indicating much superior safety performance after the construction of the double-shell structure. In general, this work has provided an effective and versatile strategy to conquer the thermal stability and safety issues of CL-20 and contributes to the future application of high energy density energetic materials.

**Keywords:** CL-20; Double-shell structure; Thermal stability; Safety performance; Tannic acid; Graphene sheets

### 1. Introduction

With the rapid development of modern weapon systems, energetic materials that possess both high detonation energy and good safety performance are in high demand [1, 2]. Hexanitrohexaazaisowurtzitane (CL-20), as the third generation of a single explosive, has attracted tremendous attention from researchers [3–8]. The superior comprehensive properties of CL-20 endow it with huge application potential for the formula design of composite explosives in the future. However, the intrinsic high sensitivity and poor thermal stability (low crystal transformation temperature) still strictly limit the practical applications of CL-20 so far.

In recent years, several strategies have been developed to inhibit the crystal transformation and decrease the sensitivity of CL-20. These include coating [9–13], doping [3, 14], co-crystallization [5, 6, 15] and recrystallization [16, 17] strategies, etc. Among those strategies, coating technology possesses the advantages of easy processing and high efficiency. Therefore, it is widely used to improve the thermal stability and safety performance of CL-20. Due to the merits of facile preparation, superior coating effect and strong interfacial interactions, the in situ polymerization of dopamine approach has been employed for coating various kinds of energetic materials including CL-20 [12, 13, 18, 19]. Yang et al. modified CL-20 crystals with polydopamine (PDA) and the phase transition temperature achieved a noticeable retardation of 11 °C for CL-20@PDA composites with about 1.1 wt% PDA coating content [13]. Pan et al. had investigated the effects of different polymer coatings on the crystal transformation of CL-20 [12], and they found that the crystal transformation temperature significantly increased about 40 °C through using dopamine polymer as the coating material. The increase of the crystal transformation temperature should be ascribed to the intensive encapsulation effect derived from the uniform and dense PDA coating layer, which can effectively restrain the volume expanding of CL-20 during crystal transition.

In addition to polymer coating materials, inorganic carbon materials were also used to enhance the safety performance of CL-20. Song et al. fabricated CL-20/rGO composites for the desensitization of CL-20 and both impact and friction sensitivity were obviously improved [9], due to the lubricating effect of rGO which can dramatically diminish hotspots under the stimuli of external force. Moreover, in order to strengthen the interface interaction between CL-20 and carbon materials, researchers have utilized unique polycations as intermediate layers to enhance the interfacial interaction between CL-20 and GO via an electrostatic self-assembly process [10, 11]. Through this method, the thermal stability and sensitivity of CL-20 composites can be further enhanced.

Despite the progresses above, some basic issues still need to be solved. The in situ polymerization of dopamine approach is time consuming (taking over several hours) which severely limits the production rate. In addition, the desensitization effects of polymer coatings to CL-20 were not as good as which of inorganic carbon materials while inorganic carbon materials are useful for decreasing the sensitivity but not helpful for improving thermal stability. In a word, to develop an effective, simple and fast preparation strategy which can simultaneously improve both the thermal stability and safety performance of CL-20 remains a challenge.

Recently, as a substitute of dopamine, the natural polyphenol tannic acid (TA) have been used to modify the surface structure of materials. The large amount of phenolic hydroxyl groups in TA allows it to coordinate with metal ions to form a metal-phenolic network [20–22]. Typically, the metal-phenolic network constructed by the chelating reaction between TA and iron (III) ions ( $\text{Fe}^{\text{III}}$ ) was demonstrated to be capable of adhering intensively to almost any substrates including bulk materials, films, and nanomaterials, etc [23, 24]. Moreover, the coating process can be completed in just a few minutes using the one-step assembly of coordination complexes, which is much faster than the traditional PDA coating strategy. In the meantime, the phenolic hydroxyl groups as well as the  $\pi$ - $\pi$  structure of TA endow it with the capability to strengthen the interfacial interactions between composites, owing to the formed hydrogen bonds and  $\pi$ - $\pi$  interactions [25, 26].

Herein, we demonstrate a simple, rapid and effective method to simultaneously improve the thermal stability and safety performance of CL-20. The coordination complexes of TA and  $\text{Fe}^{\text{III}}$  were employed to coat CL-20 through the fast one-step assembly process. The construction of TA- $\text{Fe}^{\text{III}}$  layer on the surface of CL-20 could be completed within several minutes. Our results had shown that the TA- $\text{Fe}^{\text{III}}$  layer could effectively inhibit the phase transition of CL-20 and increase the thermal stability. On the other hand, in order to further decrease the sensitivity of CL-20 composites, the nano-carbon material of graphene was incorporated to modify the CL-20/TA- $\text{Fe}^{\text{III}}$  composites. Through this simple and rapid manner, the double shell of TA- $\text{Fe}^{\text{III}}$  and graphene could be successfully constructed on the surface of CL-20 crystals. In the end, the resulting CL-20/TA- $\text{Fe}^{\text{III}}$ /graphene (denoted as CL-20/TA- $\text{Fe}^{\text{III}}$ /G) composites exhibited both superior thermal stability and safety performance. We believe that this work has provided a promising and versatile strategy for simultaneously enhancing the thermal stability and safety performance of energetic materials.

## 2. Experimental section

### 2.1. Materials

The CL-20 crystals were provided by the Institute of Chemical Materials, CAEP, China. Tannic acid (TA, ACS reagent) and iron (III) chloride hexahydrate ( $\text{FeCl}_3 \cdot 6\text{H}_2\text{O}$ ) were purchased from Sigma-Aldrich. The water soluble graphene sheets with about 5  $\mu\text{m}$  in width and 2 nm in thickness were purchased from Deyang Xitan Nano Technology Co., Ltd. China, which were shown in Fig. S1 in Supporting Information. Deionized water prepared by the purification machine was used through

the entire experimental process.

## 2.2. Preparation of CL-20/TA-Fe<sup>III</sup> composites

Firstly, 50 mL of aqueous solution consisting TA and FeCl<sub>3</sub>·6H<sub>2</sub>O were prepared in which the concentrations of TA and FeCl<sub>3</sub>·6H<sub>2</sub>O are 40 and 10 mg/mL, respectively. After vigorously stirring the solution for 1 minute, 5 grams of CL-20 crystals were added to the solution and then stirred for an additional 5 minutes. Washing and filtering the composites with deionized water repeatedly for three times. The resulting CL-20/TA-Fe<sup>III</sup> composites were obtained after drying at 60 °C in a vacuum oven for 8 hours.

## 2.3. Preparation of CL-20/TA-Fe<sup>III</sup>/G composites

The above obtained CL-20/TA-Fe<sup>III</sup> composites were added into the aqueous graphene dispersion and stirred for 5 min. After filtration and drying, the CL-20/TA-Fe<sup>III</sup>/G composites could be finally obtained. The content of graphene in the composites was fixed at 0.5 wt%. For comparison, the CL-20 crystals coated with graphene sheets alone (denoted as CL-20/G composites) were also prepared with the same preparation procedures above.

## 2.4. Characterization

The morphologies of the CL-20 crystals and composites were characterized with Field-Emission Scanning Electron Microscope (FESEM, JSM-6390LV, Zeiss). X-ray diffraction (XRD) tests were conducted using an X'Pert PRO (PANalytical) diffractometer operating at 40 kV and 40 mA with monochromatic Cu K $\alpha$  radiation ( $\lambda=1.54$  Å). Raman spectra of the composites were recorded using a 532 nm laser source (HORIBA JobinYvon XploRA) with a wave range of 500–3500 cm<sup>-1</sup>. Fourier transform infrared spectrometer (FT-IR) spectra were conducted on a Nicolet 6700 spectrometer at room temperature over a frequency range of 500–4000 cm<sup>-1</sup>. The High-performance liquid chromatography (HPLC, Elite P230, China) was conducted to determine the CL-20 content in CL-20/TA-Fe<sup>III</sup> composites. The thermal behavior of the composites was analyzed using a thermogravimetric-differential scanning calorimetry (TG-DSC) with heating rates of 5, 10, 15 and 20 K/min under nitrogen atmosphere. The impact sensitivities of the raw CL-20 and composites were tested using a Bundesanstalt für Materialprüfung (BAM) Fall hammer device.

## 3. Results and discussion

### 3.1. Construction and characterization of the double-shell structure

The construction process of the double shell of TA-Fe<sup>III</sup> and graphene on the surface of CL-20 crystals was schematically shown in Fig. 1(a). When the CL-20 crystals were added into the aqueous solution consisting of FeCl<sub>3</sub> and TA, the TA-Fe<sup>III</sup> layer could form on the surface of CL-20 quickly, which made the color of CL-20 turn from white to brown (as shown in Figs. 2(b) and 2(c)). The content of TA-Fe<sup>III</sup> layer in CL-20/TA-Fe<sup>III</sup> composites was calculated as 0.5 wt% based on the HPLC characterization (as shown in Table S1 in the Supporting Information). The limit content of TA-Fe<sup>III</sup> layer contributed to the preservation of the high detonation performance of the CL-20 composites. Due to the intensive encapsulation effect of TA-Fe<sup>III</sup> layer, the particle size of CL-20/TA-Fe<sup>III</sup> was closed to that of CL-20 (as shown in Fig. S2). With further coating of graphene sheets, the black CL-20/TA-Fe<sup>III</sup>/G composites were obtained (Fig. 1(d)). Here, large quantities of oxygen-containing groups (such as phenolic hydroxyl groups) as well as the  $\pi$ - $\pi$  structure of TA-Fe<sup>III</sup> (specified in Fig. 1(a)) contribute to form strong interfacial interactions with graphene sheets (these interactions include hydrogen bonding and  $\pi$ - $\pi$  interactions), making the interfacial interactions between CL-20 and graphene enhanced effectively, endowing the CL-20/TA-Fe<sup>III</sup>/G composites with increased particle size relative to that of raw CL-20 (Fig. S2). Through this method, the double shell of TA-Fe<sup>III</sup> and graphene could be successfully constructed on the surface of CL-20.

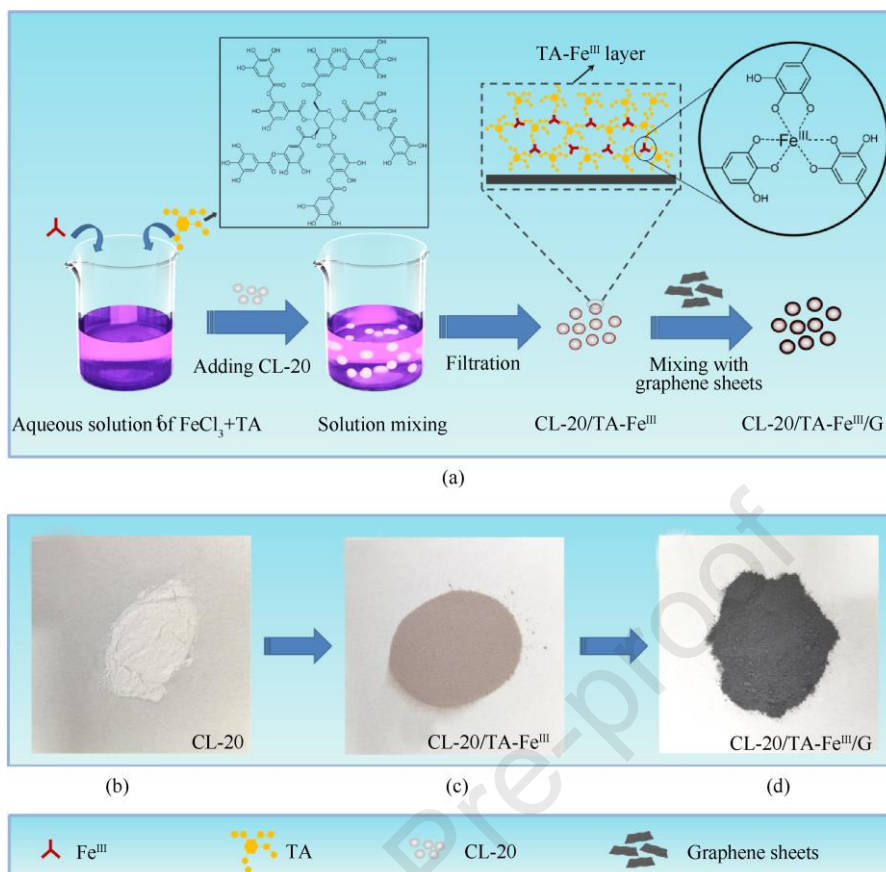


Fig. 1. Schematic diagram for the construction of a double shell consisting of TA-Fe<sup>III</sup> and graphene on the surface of CL-20 crystals.

The surface morphologies of the explosive crystals characterized by FESEM are shown in Fig. 2. The raw CL-20 crystals exhibit a relatively flat and smooth surface with clear edges (Figs. 2(a) and 2(b)). This phenomenon in the change of surface morphologies after construction of TA-Fe<sup>III</sup> was in consistent with previous reported study [24]. After modification with TA-Fe<sup>III</sup> complexes, as shown in Figs. 2(c) and 2(d), the surface morphologies of CL-20/TA-Fe<sup>III</sup> crystals turn rough and curled in which some TA-Fe<sup>III</sup> aggregates can be found (indicated by the red ovals in Fig. 2(d)). For the CL-20/G crystals, it can be seen that the explosive crystals are not well coated by the graphene sheets and a large amount of graphene sheets are separated from the crystals (indicated by the red arrows and circle in Figs. 2(e) and 2(f)) due to the weak interaction between CL-20 and graphene. In contrast, with the construction of the core@double-shell structure, the graphene sheets are tightly adhered to the explosive crystals resulting in quite coarse surface morphologies for CL-20/TA-Fe<sup>III</sup>/G composites (shown in Figs. 2(g) and 2(h)). The reason should be ascribed to the strong hydrogen bonding and  $\pi$ - $\pi$  interactions formed between graphene and TA molecules, which effectively enhance the interactions between graphene and CL-20.

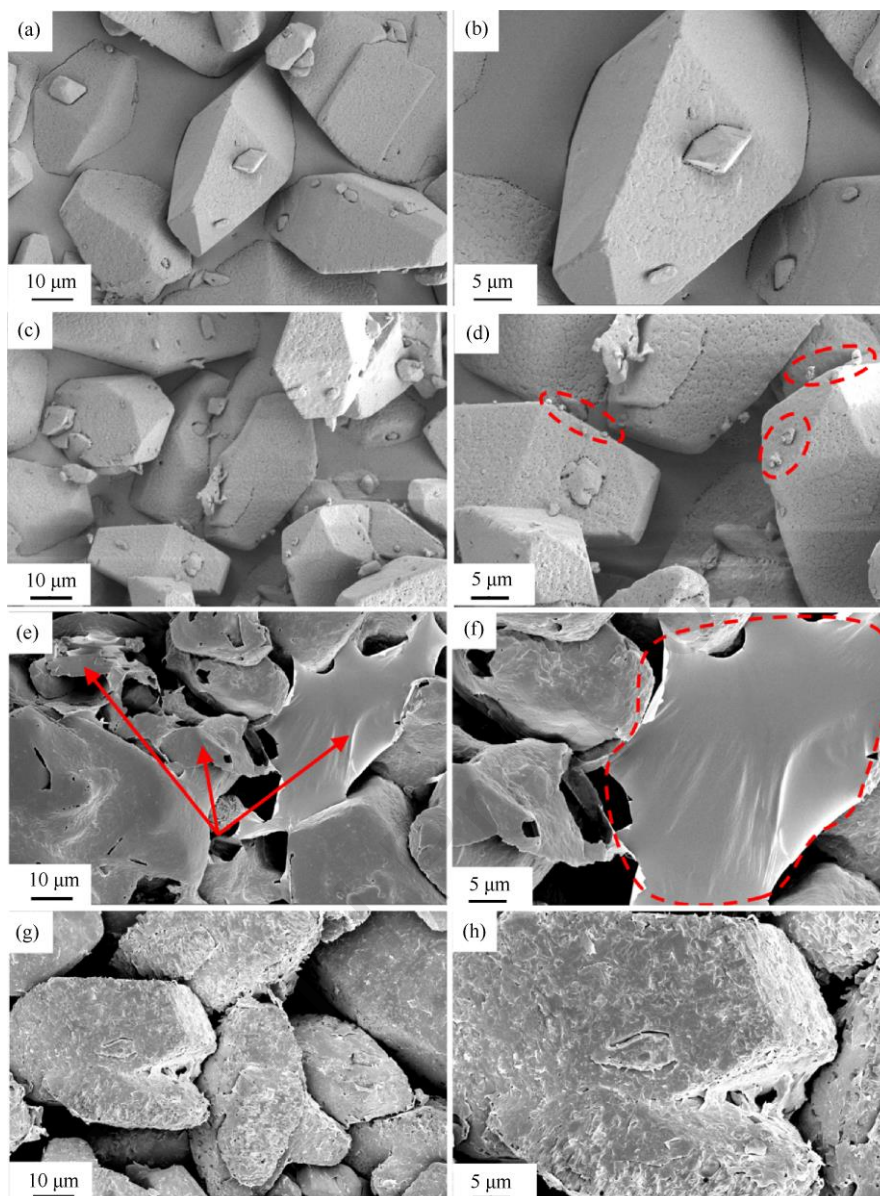


Fig. 2. FESEM images of the surface morphologies of the explosive crystals of (a, b) CL-20; (c, d) CL-20/TA-Fe<sup>III</sup>; (e, f) CL-20/G; (g, h) CL-20/TA-Fe<sup>III</sup>/G with different magnifications, respectively.

Raman spectroscopy can also provide information about the chemical structure of CL-20 during the coating process. As shown in Fig. 3(a), for raw CL-20, the characteristic peaks at about 818, 1306, 1624 and 3046  $\text{cm}^{-1}$  are ascribed to the symmetrical vibration of CL-20 skeleton, symmetric stretching vibration of nitro group, anti-symmetric stretching vibration of nitro group and stretching vibration of C-H group, respectively [4, 10]. In terms of graphene, the characteristic peaks at 1582 and 2705  $\text{cm}^{-1}$  correspond to the G and 2D band, respectively [27, 28]. While for TA-Fe<sup>III</sup>, the peaks observed around 1600 and 1700  $\text{cm}^{-1}$  indicate the ester groups and aromatic rings of TA, respectively [29]. After constructing a double shell of TA-Fe<sup>III</sup> and graphene, the intensity of the characteristic peaks of raw CL-20 was significantly weakened while the intensity of the characteristic peaks of graphene was preserved in CL-20/TA-Fe<sup>III</sup>/G composites (as indicated by the yellow region in Fig. 3(a)). Due to the enhanced interfacial interactions, the graphene sheets were tightly adhered to the surface of the CL-20 crystals in CL-20/TA-Fe<sup>III</sup>/G composites, thus, during Raman characterization, the main signal of characteristic peaks presented was for graphene.

Besides, the FT-IR spectra of the composites exhibited a similar change trend to Raman spectra (shown in Fig. S3), both of which indicate successful construction of the double shells of TA-Fe<sup>III</sup> and graphene on the surface of CL-20 crystals. Moreover, the XRD characterization was also used to investigate whether the coating process would cause a phase transition of CL-20 or not. As shown in Fig. 3(b), the corresponding energetic composites after coating exhibited similar characteristic peaks compared with which of raw CL-20, revealing that the coating process would not influence the crystal form of CL-20. This result is helpful for the modified CL-20 composites to maintain the superior detonation performance and contributes to the practical application of the coating strategy for the enhancement of thermal stability and safety performance of CL-20.

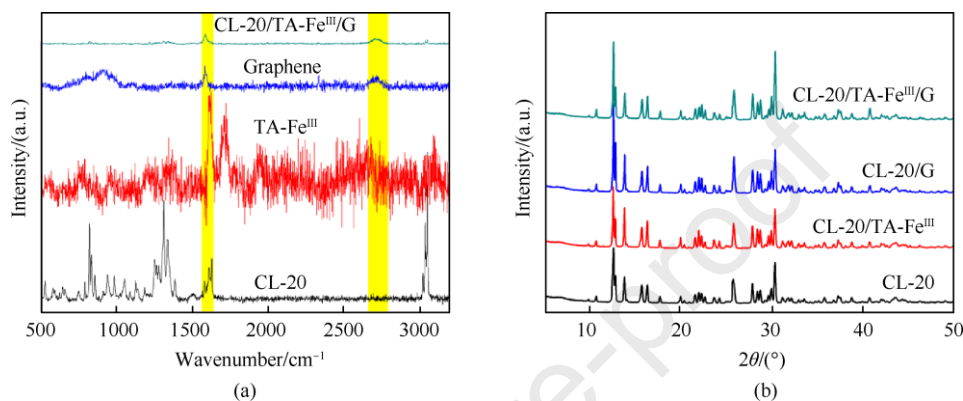


Fig. 3. (a) Raman spectra of raw CL-20, TA-Fe<sup>III</sup>, graphene and CL-20/TA-Fe<sup>III</sup>/G; (b) XRD patterns of raw CL-20, CL-20/TA-Fe<sup>III</sup>, CL-20/G and CL-20/TA-Fe<sup>III</sup>/G, respectively.

### 3.2. Thermal stability and safety performance of the modified CL-20 composites

The thermal stability of CL-20 is closely related to its reliability in use and its storage safety performance. Due to the polymorphic characteristics of CL-20, under the stimulus of high temperature condition, the phase transition of CL-20 crystal could occur, which would result in the volume expansion of CL-20 explosive. Consequently, the cracks could be generated and severely threaten the safety performance of the explosive part of weapon system. Thus, to strictly inhibit the phase transition phenomenon of CL-20 is of great importance for its practical applications. As shown in Fig. 4, the phase transition phenomenon of raw CL-20, CL-20/TA-Fe<sup>III</sup>, CL-20/G and CL-20/TA-Fe<sup>III</sup>/G happened at 173.70 °C, 182.51 °C, 173.73 °C and 192.42 °C, respectively. It signifies that coating the coordination complexes of TA-Fe<sup>III</sup> endowed the composites with a noticeable increase in phase transition temperature (about 9 °C), demonstrating the TA-Fe<sup>III</sup> coating layer presented good encapsulation effect to CL-20 and inhibited that the volume expansion during the heating process. Moreover, the coating process of TA-Fe<sup>III</sup> could be completed within several minutes (detailed information was shown in Fig. S4), which was much shorter than the commonly used in situ polymerization of dopamine approach (over several hours), indicating the high production efficiency of this coating strategy here. In comparison, coating the graphene sheets alone did not cause a observable change in the phase transition temperature, revealing the weak constraint effect of graphene to CL-20, which was possibly due to the absence of strong interactions between CL-20 and graphene sheets. Furthermore, with the construction of core@double-shell structure, the resultant CL-20/TA-Fe<sup>III</sup>/G composites exhibited a highest phase transition temperature of 192.42 °C, which was nearly 20 °C higher than that of raw CL-20. The strong interfacial interactions between TA-Fe<sup>III</sup> and graphene sheets contributed to the intense adhesion of graphene to CL-20. As a result, the encapsulation effect to CL-20 was further enhanced by the

double coating layers of TA-Fe<sup>III</sup> and graphene sheets, which should be responsible for the superior thermal stability of CL-20/TA-Fe<sup>III</sup>/G composites. In addition, the differences in thermal decomposition temperature of the energetic composites were quite small (less than 2 °C), indicating the good compatibility between the coating agents and CL-20 crystals [10, 11].

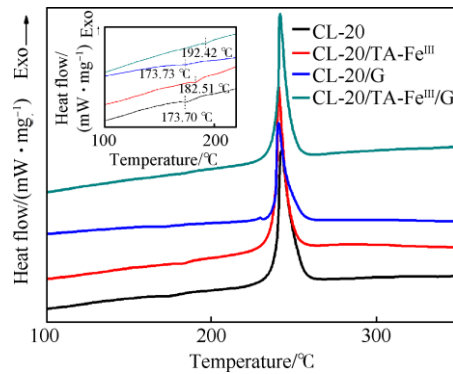


Fig. 4. DSC curves of raw CL-20, CL-20/TA-Fe<sup>III</sup>, CL-20/G and CL-20/TA-Fe<sup>III</sup>/G, respectively. The heating rate is 10 °C/min.

To further study the effect of the coating process on the thermal stability of the CL-20, the corresponding activation energy of raw CL-20 crystals and CL-20/TA-Fe<sup>III</sup>/G composites was figured out using the Kissinger-Akahira-Sunose (KAS) method. The KAS's equation is described as follows [30, 31]:

$$\ln \frac{\beta}{T_p^2} = \ln \left[ \left( \frac{R \cdot A}{E} \right) \right] - \frac{E}{R} \cdot \frac{1}{T_p}$$

where  $T_p$  is the peak temperature of the exothermic process (K),  $A$  is the pre-exponential factor,  $E$  is the activation energy (J/mol),  $R$  is the ideal gas content ( $8.314 \text{ J} \cdot \text{K}^{-1} \cdot \text{mol}^{-1}$ ) and  $\beta$  is the heating rate ( $\text{K} \cdot \text{min}^{-1}$ ). The above equation signifies that the  $\ln(\beta/T_p^2)$  and  $1/T_p$  exhibit a linear relationship. The DSC curves of CL-20 and CL-20/TA-Fe<sup>III</sup>/G under different heating rates were shown in Figs. 5(a) and 5(b). The fitted results based on the above equation were shown in Figs. 5(c) and 5(d) and the corresponding linear correlation coefficients are quite close to 1, which demonstrates the usability of the introduced KAS method. Subsequently the  $E$  values of CL-20 and CL-20/TA-Fe<sup>III</sup>/G were calculated as 231.46 and 517.51 kJ/mol, respectively. After the construction of the double shell of TA-Fe<sup>III</sup> and graphene, the activation energy of CL-20 dramatically increased, indicating much superior thermal stability of CL-20/TA-Fe<sup>III</sup>/G composites compared with that of raw CL-20 crystals. The improved thermal stability was possibly due to the intensive constraint effect resulted from the created double shell structure in this study.

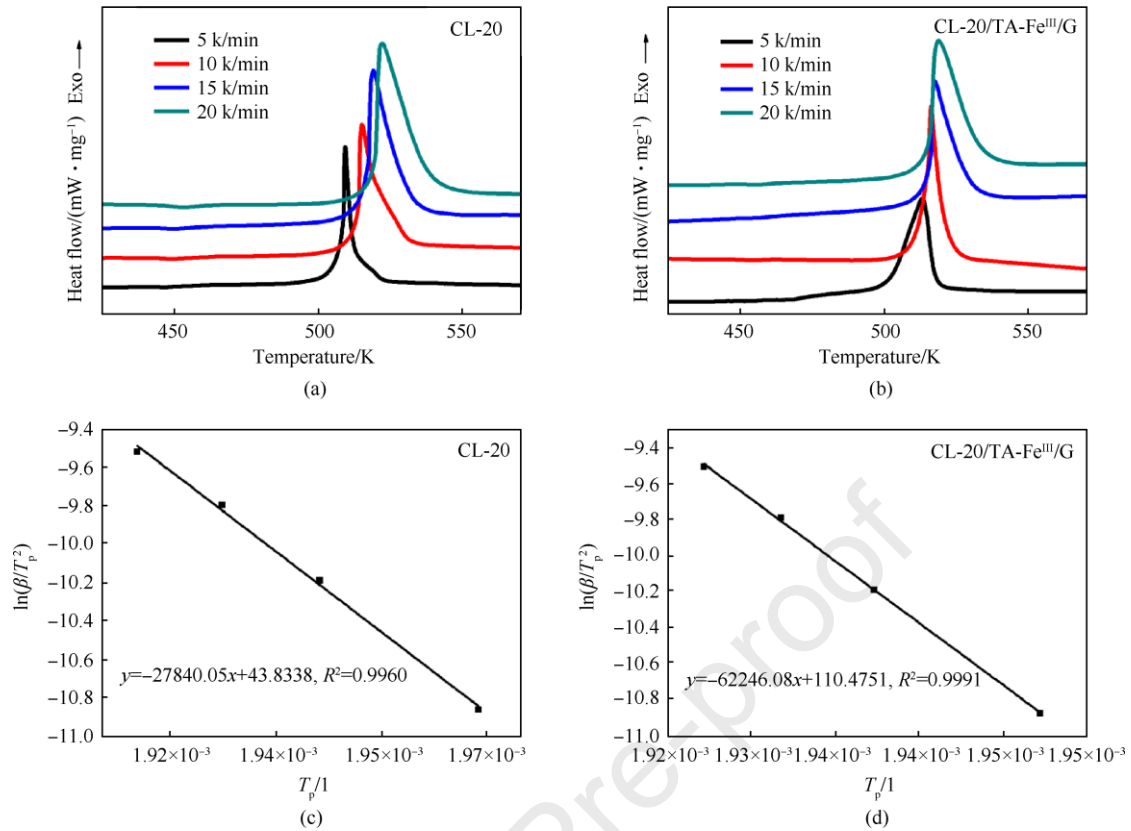


Fig. 5. DSC curves of (a) raw CL-20 and (b) CL-20/TA-Fe<sup>III</sup>/G and fitting results of (c) raw CL-20 and (d) CL-20/TA-Fe<sup>III</sup>/G with KAS method.

The high sensitivity of CL-20 was another key problem which severely hindered its practical application. Here, the desensitization effect of the constructed double shell structure to CL-20 was investigated based on the standard BAM method. As shown in Table 1, the  $H_{50}$  (characteristic drop height) of raw CL-20 was only 14.7 cm, indicating the high sensitivity of CL-20 to the external mechanical stimuli. When the TA-Fe<sup>III</sup> layer was constructed, the CL-20/TA-Fe<sup>III</sup> composites presented only a small increase in  $H_{50}$  (from 14.7 to 20.3 cm). On the other hand, when the graphene sheets were coated on the surface of CL-20, an obvious increase in  $H_{50}$  (from 14.7 to 74.2 cm) occurred for CL-20/G composites. Finally, as the double shell structure was created, the CL-20/TA-Fe<sup>III</sup>/G composites exhibited the best safety performance, for which the  $H_{50}$  was over 7 times of that of raw CL-20 and also higher than that of CL-20/G composites. The above phenomena signified that for the desensitization of CL-20, the layer of graphene sheets contributed more than the layer of TA-Fe<sup>III</sup>, which was mainly ascribed to the lubrication effect of graphene sheets on CL-20 under external mechanical stimuli. In terms of TA-Fe<sup>III</sup> layer, it successfully acted as a link bridge (as shown in Fig. 6) which largely enhanced the interfacial interactions between graphene sheets and CL-20, endowing the CL-20/TA-Fe<sup>III</sup>/G composites with superior desensitization effect to that of CL-20/G composites.

Table 1

The impact sensitivity of raw CL-20 and the corresponding composites.

Sample	$H_{50}$ /cm
CL-20	14.7
CL-20/TA-Fe <sup>III</sup>	20.3

CL-20/G	74.2
CL-20/TA-Fe <sup>III</sup> /G	112.8

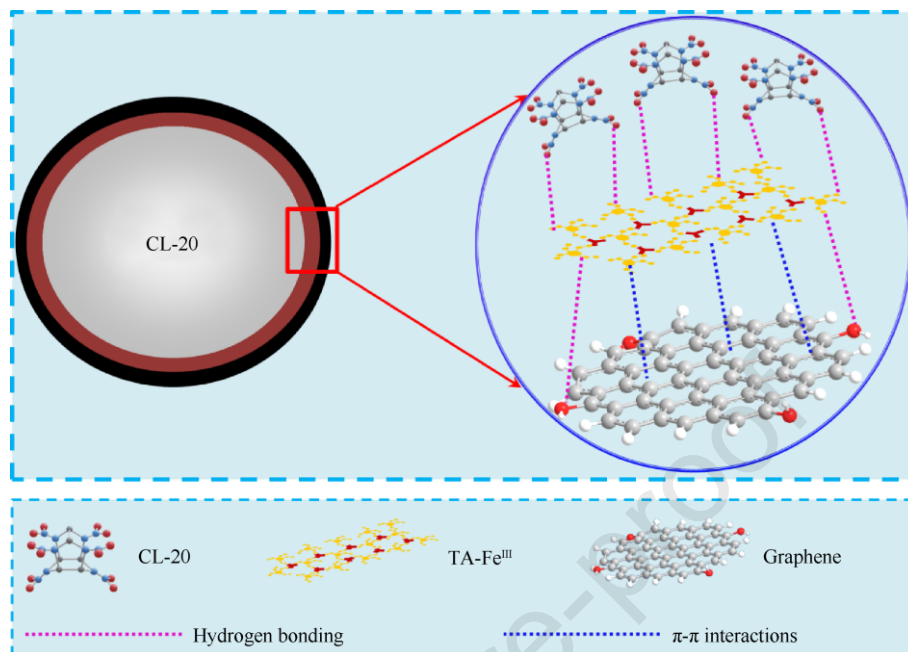


Fig. 6. Schematic of the link bridge function of TA-Fe<sup>III</sup> to enhance the interfacial interactions between CL-20 and graphene sheets.

### 3.3. Interaction behaviors among the interfaces of CL-20, TA-Fe<sup>III</sup> and graphene

In order to further specify the interfacial interactions among CL-20, TA-Fe<sup>III</sup> and graphene shell quantitatively, the molecular models for graphene as well as TA-Fe<sup>III</sup> segments were constructed and optimized using molecular mechanics, as shown in Figs. 7(a) and 7(b). The  $3 \times 3 \times 2$  super cell of  $\epsilon$ -CL-20 was constructed and cleaved along two main crystalline directions (0 0 2) and (0 2 0) [32]. Then graphene with density of 2.2 g/cm<sup>3</sup> and TA-Fe<sup>III</sup> segment with density of 2.12 g/cm<sup>3</sup> were put onto the CL-20 surfaces respectively to form interface models, as shown in Figs. 7(c) and 7(d). Besides, the interface model of graphene and TA-Fe<sup>III</sup> was also constructed, as shown in Fig. 7(e). All the interface models were geometric optimized and energy minimized using molecular mechanics. Consequently, molecular dynamics simulation under the ensemble of constant particle number, volume and temperature (NVT) and COMPASS force field were performed on the interface models at normal temperature of 298 K [33, 34]. Each simulation lasted 500 ps to ensure the equilibrium of both energy and temperature.

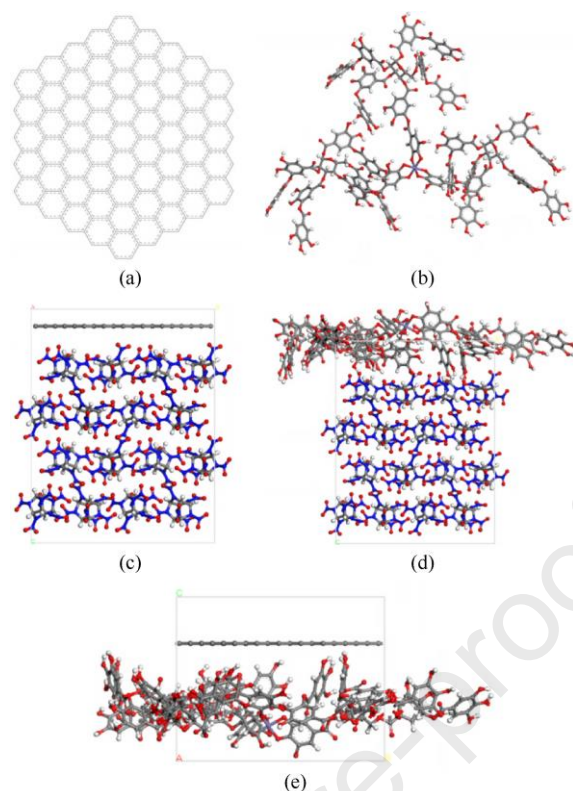


Fig. 7. (a) Molecular models for graphene segment; (b) TA-Fe<sup>III</sup> segment; (c) Graphene segment on CL-20 (0 0 2) surface [G-CL-20 (0 0 2)]; (d) TA-Fe<sup>III</sup> segment on CL-20 (0 0 2) surface [TA-Fe<sup>III</sup>-CL-20 (0 0 2)]; (e) Graphene on TA-Fe<sup>III</sup> (G-TA-Fe<sup>III</sup>).

The calculated interface energy ( $E_{inter}$ ) as well as the contribution of van der Waals force (vdW) and electrostatic interaction (ES) based on the above models are shown in Table 2 [35]. It can be seen that, the interaction energy between TA-Fe<sup>III</sup> and CL-20 interface is much stronger than that between graphene and CL-20 interface, directly demonstrating the intensive constraint effect of TA-Fe<sup>III</sup> coating layer on CL-20 crystal. The greatly enhanced interaction energy between TA-Fe<sup>III</sup> and CL-20 interface, compared with that between graphene and CL-20 interface, is mainly ascribed to the much stronger vdW as well as the ES and for the latter, there is almost no ES. The reason can be concluded as the abundant phenolic hydroxyl groups in TA-Fe<sup>III</sup> can interact with the nitro groups in CL-20, forming large quantities of relatively strong interactions such as hydrogen bonds, then obviously strengthening the interfacial interactions. What is more, the interaction energy between graphene and TA-Fe<sup>III</sup> is also stronger than that between graphene and CL-20, signifying that the TA-Fe<sup>III</sup> segment can act as a link bridge to increase the interfacial interactions between graphene and CL-20, which is helpful for further improving both the physical constraint and desensitization effects of the constructed double shell structure on CL-20 crystals.

Table 2

Interaction energy for the different interfaces.

System	$E_{inter}/(\text{kcal}\cdot\text{mol}^{-1})$	vdW/ $(\text{kcal}\cdot\text{mol}^{-1})$	ES/ $(\text{kcal}\cdot\text{mol}^{-1})$
G-CL-20 (0 0 2)	-142.83	-136.53	0.00
G-CL-20 (0 2 0)	-97.00	-91.67	0.00
TA-Fe <sup>III</sup> -CL-20 (0 0 2)	-559.89	-252.66	-291.31
TA-Fe <sup>III</sup> -CL-20 (0 2 0)	-477.67	-233.46	-230.06

G-TA-Fe <sup>III</sup>	-173.64	-171.55	0.00
------------------------	---------	---------	------

#### 4. Conclusions

Here we have successfully constructed a double-shell structure on the surface of CL-20 crystals which improved the thermal stability and safety performance of CL-20 simultaneously. The inner shell of TA-Fe<sup>III</sup> mainly contributed to inhibiting the phase transition phenomenon of CL-20 under high temperature conditions while the outer shell of graphene sheets mainly exhibited a desensitization effect on CL-20. Moreover, owing to the link bridge function of TA-Fe<sup>III</sup> which largely increases the interfacial interactions between graphene sheets and CL-20, a synergistic enhancement effect occurred in the thermal stability and safety performance of the final CL-20/TA-Fe<sup>III</sup>/G composites. The corresponding phase transition temperature, H<sub>50</sub> and activation energy had dramatically increased to 192.42 °C, 112.8 cm and 517.51 kJ/mol, which were about 20 °C, over 6 times and 286 kJ/mol higher than those of raw CL-20 crystals and also much superior to the performance of CL-20/TA-Fe<sup>III</sup> and CL-20/G composites. In addition, the coating process of TA-Fe<sup>III</sup> complexes could be completed within only 5 min, which was much quicker than the traditional PDA coating strategy and greatly sped up the production rate of the final composites. We believe this effective, simple and fast preparation strategy is quite promising for simultaneously enhancing the thermal stability and safety performance of energetic materials with high energy density and contributing to their practical applications.

#### Acknowledgment

This work was financially supported by the National Natural Science Foundation of China (Grant No. 22275173) and the Open Project of State Key Laboratory of Environment-friendly Energy Materials (Grant No. 22kfhg10).

#### References

- [1] Yan T, Yang C, Ma J, Cheng G, Yang H. Intramolecular integration of multiple heterocyclic skeletons for energetic materials with enhanced energy & safety. *Chem. Eng. J.* 2022; 428: 131400.
- [2] Chiquete C, Jackson S, Anderson E, Short M. Detonation performance experiments and modeling for the DAAF-based high explosive PBX 9701. *Combust. Flame* 2021; 223: 382-397.
- [3] Huang B, Xue Z, Chen S, Chen J, Li X, Xu K, Yan Q. Stabilization of  $\epsilon$ -CL-20 crystals by a minor interfacial doping of polydopamine-coated graphene oxide. *Appl. Surf. Sci.* 2020; 510: 145454.
- [4] Chen T, Zhang Y, Guo S, Zhao L, Chen W, Hao G, Xiao L, Ke X, Jiang W. Preparation and property of CL-20/BAMO-THF energetic nanocomposites. *Def. Technol.* 2019; 15: 306-312.
- [5] Wu Z, Liu N, Zheng W, Chen J, Song X, Wang J, Cui C, Zhang D, Zhao F. Application and properties of CL-20/HMX cocrystal in composite modified double base propellants. *Propellants Explos. Pyrotech.* 2020; 45: 92-100.
- [6] Zhou J, Shi L, Zhang C, Li H, Chen M, Chen W. Theoretical analysis of the formation driving force and decreased sensitivity for CL-20 cocrystals. *J. Mol. Struct.* 2016; 1116: 93-101.
- [7] Wei Y, Wang J, An C, Li H, Wen X, Yu B. GAP/CL-20-based compound explosive: A new booster formulation used in a small-sized initiation network. *J. Energetic Mater.* 2017; 35: 53-62.
- [8] Tang X, Zhu R, Shi T, Wang Y, Niu X, Zhang Y, Zhu J, Li W, Hu W, Xu R. Research progress and key issues of hydrodebenzylation of hexabenzylhexaazaisowurtzitane (HBIW) in the synthesis of

- high energy density material hexanitrohexaazaisowurtzitane (HNIW). *Materials* 2022; 15: 409.
- [9] Song X, Huang Q, Jin B, Peng R. Preparation of desensitizing CL-20/rGO composites by in-situ reduction. *Propellants Explos. Pyrotech.* 2020; 45: 1293-1299.
- [10] Song X, Huang Q, Jin B, Peng R. Fabrication and characterization of CL-20/PEI/GO composites with enhanced thermal stability and desensitization via electrostatic self-assembly. *Appl. Surf. Sci.* 2021; 558: 149933.
- [11] Song Y, Huang Q, Jin B, Peng R. Electrostatic self-assembly desensitization of CL-20 by enhanced interface interaction. *J. Alloy. Compd.* 2022; 900: 163504.
- [12] Pan Q, Zhang H, Guo X, Zhao W, Fan X. Effects of different coatings on the crystal transformation of  $\beta$ -HNIW. *J. Cryst. Growth* 2021; 566-567: 126175.
- [13] Yang X, Gong F, Zhang K, Yang W, Zeng C, Yang Z. Enhanced creep resistance and mechanical properties for CL-20 and FOX-7 based PBXs by crystal surface modification. *Propellants Explos. Pyrotech.* 2021; 46: 572-578.
- [14] Hao M, Chi W, Tian M, Li Z. Effect of nitrogen-doping on detonation and stability properties of CL-20 derivatives from a theoretical viewpoint. *Propellants Explos. Pyrotech.* 2017; 42: 1044-1050.
- [15] Herrmannsdörfer D, Stierstorfer J, Klapötke T. Solubility behaviour of CL-20 and HMX in organic solvents and solvates of CL-20. *Energetic Materials Frontiers* 2021; 2: 51-61.
- [16] Urbelis J, Swift J. Solvent effects on the growth morphology and phase purity of CL-20. *Cryst. Growth Des.* 2014; 14: 1642-1649.
- [17] Wei X, Xu J, Li H, Long X, Zhang C. Comparative study of experiments and calculations on the polymorphisms of 2,4,6,8,10,12-hexanitro-2,4,6,8,10,12-hexaazaisowurtzitane (CL-20) precipitated by solvent/antisolvent method. *J. Phys. Chem. C* 2016; 120: 5042-5051.
- [18] He G, Yang Z, Pan L, Zhang J, Liu S, Yan Q. Bioinspired interfacial reinforcement of polymer-based energetic composites with a high loading of solid explosive crystals. *J. Mater. Chem. A* 2017; 5: 13499-13510.
- [19] Lin C, Huang B, Gong F, Yang Z, Liu J, Zhang J, Zeng C, Li Y, Li J, Guo S. Core@double-shell structured energetic composites with reduced sensitivity and enhanced mechanical properties. *ACS Appl. Mater. Interfaces* 2019; 11: 30341-30351.
- [20] Ejima H, Richardson J, Caruso F. Metal-phenolic networks as a versatile platform to engineer nanomaterials and biointerfaces. *Nano Today* 2017; 12: 136-148.
- [21] Guo J, Ping Y, Ejima H, Alt K, Meissner M, Richardson J, Yan Y, Peter K, Elverfeldt D, Hagemeyer C, Caruso F. Engineering multifunctional capsules through the assembly of metal-phenolic networks, *Angew. Chem. Int. Ed.* 2014; 53: 5546-5551.
- [22] Rahim M, Kristufek S, Pan S, Richardson J, Caruso F. Phenolic building blocks for the assembly of functional materials, *Angew. Chem. Int. Ed.* 2019; 58: 1904-1927.
- [23] Ejima H, Richardson J, Liang K, Best J, Koeverden M, Such G, Cui J, Caruso F. One-step assembly of coordination complexes for versatile film and particle engineering. *Science* 2013; 341: 154-157.
- [24] Mao C, Qu Y, Wang J, Xu R, Huang J, Yin H. Strengthening and toughening energetic polymer composites via assembly of metal-phenolic network. *Compos. Sci. Technol.* 2022; 226: 109546.
- [25] Liu B, Wang Y, Miao Y, Zhang X, Fan Z, Singh G, Zhang X, Xu K, Li B, Hu Z, Xing M. Hydrogen bonds autonomously powered gelatin methacrylate hydrogels with super-elasticity, self-heal and underwater self-adhesion for sutureless skin and stomach surgery and E-skin. *Biomaterials* 2018; 171: 83-96.

- [26] Sun C, Xiong B, Pan Y, Cui H. Adsorption removal of tannic acid from aqueous solution by polyaniline: analysis of operating parameters and mechanism. *J. Colloid Interf. Sci.* 2017; 487: 175-181.
- [27] Yitzhak N, Girshevitz O, Fleger Y, Haran A, Katz S, Butenko A, Kaveh M, Shlimak I. Analysis of fluctuations in the Raman spectra of suspended and supported graphene films. *Appl. Surf. Sci.* 2021; 536: 147812.
- [28] Vincent T, Kawahara K, Antonov V, Ago H, Kazakova O. Data cluster analysis and machine learning for classification of twisted bilayer graphene. *Carbon* 2023; 201: 141-149.
- [29] Moghaddam P, Amini R, Kardar P, Ramezanzadeh B. Synergistic corrosion inhibition effects of the non-hazardous cerium nitrate and tannic acid polyphenolic molecules on the surface of mild-steel in chloride-containing solution: Detailed surface and electrochemical explorations. *J. Mol. Liq.* 2021; 322: 114510.
- [30] Yang Q, Chen S, Xie G, Gao S. Synthesis and characterization of an energetic compound  $\text{Cu}(\text{Mtta})_2(\text{NO}_3)_2$  and effect on thermal decomposition of ammonium perchlorate. *J. Hazard. Mater.* 2011; 197: 199-203.
- [31] Li L, Sun X, Qiu X, Xu J, Li G. Nature of catalytic activities of CoO nanocrystals in thermal decomposition of ammonium perchlorate. *Inorg. Chem.* 2008; 47: 8839-8846.
- [32] Nielsen A, Chafin A, Christian S, Moore D, Nadler M, Nissan R, Vanderah D, Gilardi R, George C, Anderson J. Synthesis of polyazapolycyclic caged polynitramines. *Tetrahedron* 1998; 54: 11793-11812.
- [33] Nosé S. A molecular dynamics method for simulations in the canonical ensemble. *Mol. Phys.* 1984; 52: 255-268.
- [34] Sun H. COMPASS: an ab initio force-field optimized for condensed-phase applications - overview with details on alkane and benzene compounds. *J. Phys. Chem. B* 1998; 102: 7338.
- [35] Qiu L, Xiao H. Molecular dynamics study of binding energies, mechanical properties, and detonation performances of bicyclo-HMX-based PBXs. *J. Hazard. Mater.* 2009; 164: 329-336.

## **Conflict of Interest**

We wish to draw the attention of Editor the following facts which might be considered as potential conflicts of interest.

We confirm that the manuscript has been read and approved by all named authors. We further confirm that the order of all authors listed in the manuscript has been confirmed by all of us.

We confirm that we have given due consideration to the protection of intellectual property associated with this work.

Overall, we state that “there is no conflict of interest to declare”.

Yours sincerely,

All authors